

## Article

# Preparation of Silicon Carbide Powder from Amorphous Silica and Investigation of Synthesis Mechanism

Xuqin Duan <sup>1,2,\*</sup>, Shuaiyu Lu <sup>1</sup>, Xiaocui Jiang <sup>1</sup>, Tong Liu <sup>1</sup> and Huifen Yang <sup>1,2</sup>

<sup>1</sup> Department of Mineral Processing Engineering, School of Civil and Resource Engineering, University of Science & Technology Beijing, Beijing 100083, China; m202320108@xs.ustb.edu.cn (S.L.); jiangxc652@163.com (X.J.); 15840320630@163.com (T.L.); yanghf145@163.com (H.Y.)

<sup>2</sup> State Key Laboratory for Efficient Mining of Metal Mines, University of Science & Technology Beijing, Beijing 100083, China

\* Correspondence: dxq918@ustb.edu.cn

**Abstract:** An innovative process for preparing silicon carbide (SiC) from acid leaching residue of ferronickel slag through a carbon–thermal reduction process was proposed in this study. The results indicate that the acid leaching residue is an ideal silicon source for SiC preparation according to its high amorphous silica content of 84.20% and fine particle size of  $d_{50} = 29.16 \mu\text{m}$ . Compared with carbon black, activated carbon, and graphite, coke is the more appropriate carbon source for SiC preparation. A micron-size SiC powder with grade of 88.90% and an average particle size ( $d_{50}$ ) of  $44.68 \mu\text{m}$  can be obtained under the following conditions: the mass ratio of coke to leaching residue as 1.2:1, in an air atmosphere, reducing at  $1600 \text{ }^\circ\text{C}$  for 3 h, following by decarbonizing at  $700 \text{ }^\circ\text{C}$  for 4 h. The XRD, SEM and FTIR analyses show that the prepared powder is 3C-SiC and belongs to the  $\beta$ -SiC crystal type. Based on thermodynamic analysis and micromorphology observation, it can be concluded that with amorphous silica as the silicon source, the carbon–thermal synthesis of SiC powder follows both the solid–solid reaction mechanism and the gas–solid mechanism. The SiC created through solid–solid reaction is primarily nucleated in situ on amorphous  $\text{SiO}_2$ , with a size close to that of the original acid-leaching slag, while the SiC generated according to the gas–solid mechanism mainly nucleates heterogeneously on the surface of carbon particles, resulting in a smaller particle size and mostly adhering to the surface of solid–solid nucleated SiC particles. This study provides a feasible method for the effective utilization of amorphous silica, which is also significant for the efficient consumption of the vast acid leaching residue.

**Keywords:** silicon carbide preparation; amorphous silica; carbon–thermal reduction method



**Citation:** Duan, X.; Lu, S.; Jiang, X.; Liu, T.; Yang, H. Preparation of Silicon Carbide Powder from Amorphous Silica and Investigation of Synthesis Mechanism. *Minerals* **2024**, *14*, 189. <https://doi.org/10.3390/min14020189>

Academic Editor: Kenneth N. Han

Received: 14 December 2023

Revised: 23 January 2024

Accepted: 29 January 2024

Published: 11 February 2024



**Copyright:** © 2024 by the authors. Licensee MDPI, Basel, Switzerland. This article is an open access article distributed under the terms and conditions of the Creative Commons Attribution (CC BY) license (<https://creativecommons.org/licenses/by/4.0/>).

## 1. Introduction

Ferronickel slag, ranked as the fourth most abundant industrial solid waste slag in China, following iron slag, steel slag and red mud [1], has gained significant attention in recent years due to its ecofriendly status, efficiency, and resource utilization. Numerous studies have focused on the utilization of ferronickel slag as a raw material for crafting building materials [2], glass ceramics [3] and refractory materials [4]. Nevertheless, ferronickel slag, especially electric slag, possesses characteristics such as low calcium content and high magnesium content, which give it low gelling activity and poor stability. Additionally, the inconspicuous granulation characteristics of ferronickel slag leads to high energy consumption during grinding, thus imposing limitations on its application within the construction materials domain. Mg, Si and Fe constitute the primary valuable elements within ferronickel slag, with Si and Mg collectively accounting for approximately 80% of the total composition, while Fe comprises around 10%. The contents of other metal elements, including Ni, Cr, Al, and Ca, are comparably low [5]. The low recycling value of metal elements is also a challenge in the upgraded recovering and qualified utilizing of ferronickel slag. Acid leaching has been proven to be an efficient method for extracting

metals such as Cr [6], Ni [7,8], Fe [9] and Mg [10], and various other metallic elements from solid resources. However, acid leaching is inevitably accompanied by a large number of leaching residues. The recycling of acid leaching residues not only affects the overall cost of the acid leaching process, restricting the industrialization of the process, but is also closely related to secondary pollution control.

Owing to its favorable mechanical properties, silicon carbide (SiC) is widely used in the production of functional ceramics [11–13], high-grade refractories [13,14], abrasives [15], and metallurgical raw materials [16]. The synthesis of SiC powder is categorized into three processes based on the initial raw material states: the solid phase method, the liquid phase method, and the gas phase method [17]. Carbon–thermal reduction is a solid phase synthesis method that was pioneered in the mid-20th century, which uses a high-purity carbon source and silicon source to melt at high temperatures to prepare SiC materials. The thermal reduction method boasts significant merits, including a wide range of raw material sources, low production expenses, uncomplicated procedures, elevated product qualification rate, stable quality, and suitability for large-scale production. Consequently, the carbon–thermal reduction technique assumes a crucial role within the realm of SiC preparation [18,19]. However, the powder yielded through thermal reduction tends to lack the desired fineness, and its purity is substantially influenced by the characteristics and purity level of raw material, which represents the primary drawback of the carbon–thermal reduction process.

The selection of a carbon source and a silicon source is very important for the preparation of SiC powder, and the reactivity, purity, particle size, price and other factors should be taken into account [20]. The carbon sources commonly used in industrial production include petroleum coke, coal coke and anthracite, etc., while the silicon sources are mainly silica and quartz sand [21]. In laboratory settings, the most commonly used silicon sources are expensive high-purity Si or SiO<sub>2</sub>, and the quality requirements for carbon sources are also rigorous [22]. Lu et al. [23] used high-purity quartz sand and semi-char of tire to prepare β-SiC via the carbothermal reduction method, and the crystallinity of the obtained SiC is relatively complete. The chemical composition of the acid leaching residue of ferronickel slag is primarily Si and O, and its dominant mineral phase is amorphous silicon dioxide, which is more chemically reactive than quartz. In consequence, an acid leaching residue represents an ideal silicon source with a low cost [24]. In this research, the preparation of SiC powder via the carbothermal reduction process was investigated, using an acid leaching residue of ferronickel slag as the Si source, and coke, activated carbon, graphite and carbon black as the carbon sources, respectively. The influence of raw material and process parameters on SiC preparation was discussed to explore the synthesis mechanism and find the optimum condition. This study presents a facile route for the recycling of acid leaching waste residue, which is also conducive to improving the leaching process of ferronickel slag for extracting Mg, Fe and other valuable metals.

## 2. Materials and Methods

### 2.1. Materials

The ferronickel slag used in the study was sourced from an electric furnace nickel–iron smelter in Tangshan, Hebei Province, China; graphite powder was obtained from Henan Liugong Graphite Apparatus Co., Ltd., Zhengzhou, China; coke was derived from a coking plant in Shanxi Province; activated carbon was procured from Tianjin Guangfu Technology Development Apparatus Co., Ltd., Tianjin, China; and carbon black was acquired from Tianjin Huaran Chemical Technology Apparatus Co., Ltd., Tianjin, China.

### 2.2. Ferronickel Slag Acid Leaching Process

The process for extracting Mg and Fe from ferronickel slag by sulfuric acid under atmospheric pressure is shown in Figure 1 [10]. The conditions for the first stage of leaching are as follows: a grinding fineness of  $-0.074$  mm accounted for 94.5%, at a leaching temperature of 96 °C, acid concentration of 2.4 mol/L, liquid to solid ratio of 6:1, leaching

time of 120 min, and stirring speed of 200 r/min. The second stage leaching conditions were as follows: the temperature as 95 °C, the acid concentration was 2.4 mol/L, the liquid to solid ratio was 3:1, and the reaction time was 150 min. The resulting secondary acid leaching residue served as the silicon raw material of this study. However, this study exclusively focuses on the preparation and purification of SiC powder.

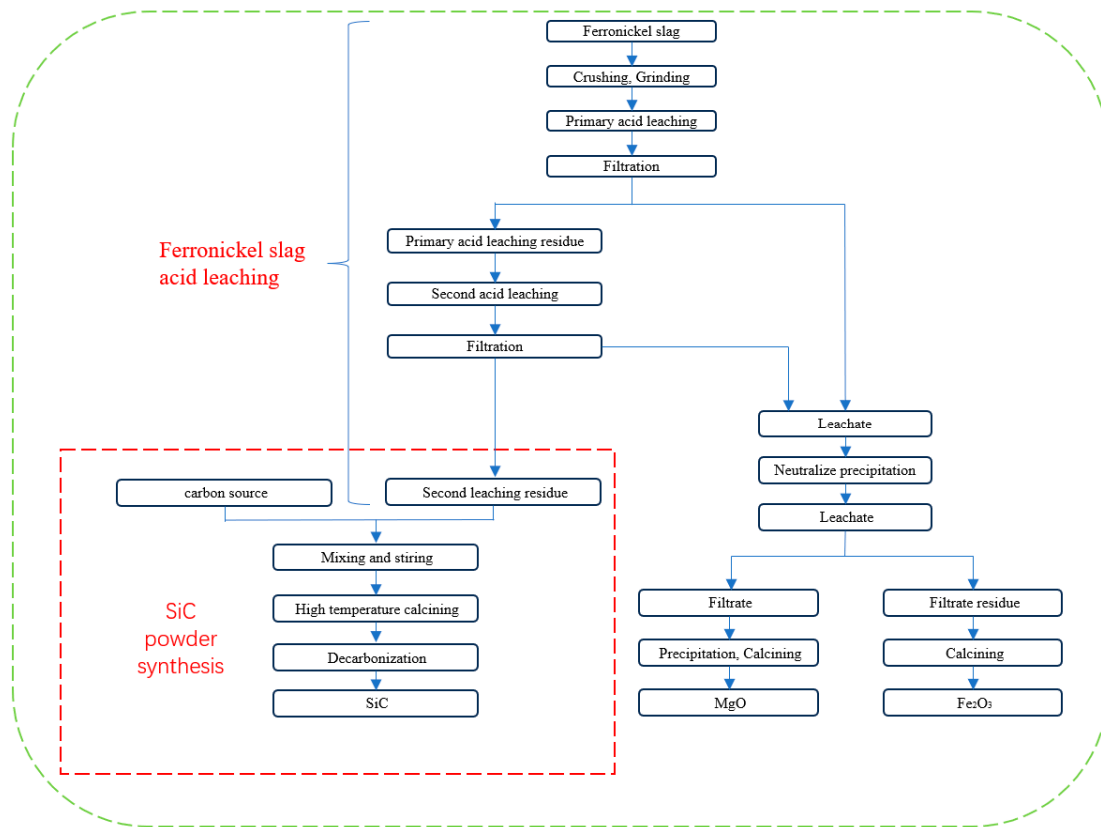


**Figure 1.** The process for extracting Mg/Fe and synthesizing SiC powder from ferronickel slag.

### 2.3. SiC Powder Synthesis

The flowsheet of the SiC powder's preparation is shown in Figure 1. Firstly, the acid leaching residue and carbon source were thoroughly mixed in a specific proportion, followed by slight grinding and stirring well. Secondly, the mixture was placed in a high-aluminum crucible and covered with an additional carbon source to consume the oxygen in the crucible and insulate the air during the reaction. Subsequently, the crucible was positioned within the Muffle furnace. The furnace temperature was set to 1500~1700 °C, and the heating rates were configured as follows: 0~1000 °C at 10 °C/min, 1000~1400 °C at 5 °C/min, and above 1400 °C at 2 °C/min. Once the designated temperature was reached, continuous heating was applied for 5 h followed by cooling to room temperature in the furnace, resulting in the production of crude SiC powder. Then, the crude SiC powder underwent decarbonation through calcination within the Muffle furnace. Finally, the finished SiC powder was prepared. The optimal decarbonation condition was ascertained based on alterations in the loss on ignition (LOI) [25] of the powder post-calcination. The calculation formula of loss on ignition is as follows:

$$\text{LOI} = \frac{M_1 - M_2}{M_1} \times 100\% \quad (1)$$

where  $M_1$  represents the sample weight before calcination (g), and  $M_2$  represents the sample weight after calcination (g).

#### 2.4. Characterization Method

Granular analysis was performed using a laser particle size analyzer model LS-POP (9) manufactured by Shanghai Jingxue Science Apparatus Co., Ltd., Shanghai, China. The tested powder was initially prepared into an aqueous suspension with a concentration of 0.01%, then dispersed by ultrasonic waves, and finally the distribution of the particle size was determined using a laser particle size analyzer (BT-9300H, Dandong Baite Products Co., Ltd., Liaoning, China).

The mineral phase analysis was performed using an X-ray diffractometer of Ultima IV type produced by Nippon Rigaku (XRD) (Tokyo, Japan). Test conditions: Cu target K $\alpha$  rays ( $\lambda = 15.406$  nm), scanning range  $2\theta = 10^\circ \sim 100^\circ$ , step size  $0.026^\circ$ , scanning speed  $20^\circ/\text{min}$ , tube current 40 mA, tube voltage 40 kV. MDI jade 6.5 was used for the analysis of the physical phase.

The microcosmic morphological characteristics of samples were analyzed using a ZEISS Gemini 300 scanning electron microscope (SEM) from Carl Zeiss Microscopy, (Oberkochen, Germany), and the elemental composition was analyzed with an energy-dispersive X-ray spectroscopy (EDS) detector (Bruker XFlash Detector 5010, Oberkochen, Germany). The acceleration voltage was 3 kV for the morphology and 15 kV for the energy spectrum, and the detector was a SE2 secondary electron detector.

The determination of organic functional groups in the powder was carried out via Fourier transform infrared spectroscopy (Nicolet iS5 FTIR, Thermo Fisher Scientific, Waltham, MA, USA). The power was 900 W. The detection range was  $350\text{--}8000\text{ cm}^{-1}$  with a maximum resolution of  $2\text{ cm}^{-1}$ .

The semi-quantitative analysis of the samples was conducted using X-ray fluorescence spectroscopy analysis (XRF-1800, Shimadzu Corporation, Kyoto, Japan) with a Rh target, operating at a maximum power of 60 kV, 140 mA and a scanning speed of  $300^\circ/\text{min}$ . The carbon contents of samples were determined using an Elementar Vario EL cube element analyzer (Elementar Analysensysteme GmbH, Frankfurt, Germany). The sample was burned at a high temperature and the element under test was converted into a gas, which was analyzed by adsorption and desorption through blowing–trapping on three special columns and then detected using a Thermal Conductivity Detector.

The samples were analyzed by thermo-gravimetry analysis (TG) and differential scanning calorimetry (DSC) using a Mettler TGA/DSC3+ simultaneous thermal analyzer (Mettler Toledo, Zurich, Switzerland). The test conditions were as follows: test temperature range from room temperature to  $800^\circ\text{C}$ , with a temperature rate of  $10^\circ\text{C}/\text{min}$  under an air atmosphere.

### 3. Result and Discussion

#### 3.1. Sample Properties Analysis

The XRF and XRD analysis results of ferronickel slag before and after acid leaching are shown in Table 1 and Figure 2, respectively. Prior to acid leaching, the ferronickel slag exhibited high Mg and Si contents, with Fe following closely, indicating a potential recyclable resource. After the two-stage acid leaching,  $\text{SiO}_2$  became the main component of the leaching slag, and the metal content was fairly low, presenting a potential silica source for SiC preparation. Comparing the XRD spectra of ferronickel slag and leaching residues, we see that the diffraction peak intensity of forsterite in the primary acid leaching residue was obviously weakened, and some weak diffraction peaks even disappeared. A distinct broad hump appeared in the  $20^\circ\text{--}40^\circ$  range, indicating that amorphous silica appeared. After two-stage acid leaching, the broad hump of amorphous silica in the leaching residue became highly pronounced, with no other detected diffraction peaks, which suggests that the dominant component of the secondary acid leaching residue is amorphous  $\text{SiO}_2$ .

**Table 1.** XRF analysis of ferronickel slag and two stage acid leaching residue (wt. %).

Oxide	SiO <sub>2</sub>	CaO	MgO	Fe <sub>2</sub> O <sub>3</sub>	Al <sub>2</sub> O <sub>3</sub>	Cr <sub>2</sub> O <sub>3</sub>	MnO	TiO <sub>2</sub>	K <sub>2</sub> O	Na <sub>2</sub> O	NiO	Others
Ferronickel Slag	44.394	4.893	36.182	8.263	4.314	0.982	0.494	0.124	0.103	0.114	0.043	0.094
The primary residue	80.732	5.714	4.172	4.168	3.556	0.687	0.315	0.154	0.119	0.112	0.024	0.247
The secondary residue	84.204	5.536	2.278	3.323	3.144	0.593	0.269	0.114	0.113	0.094	0.013	0.319

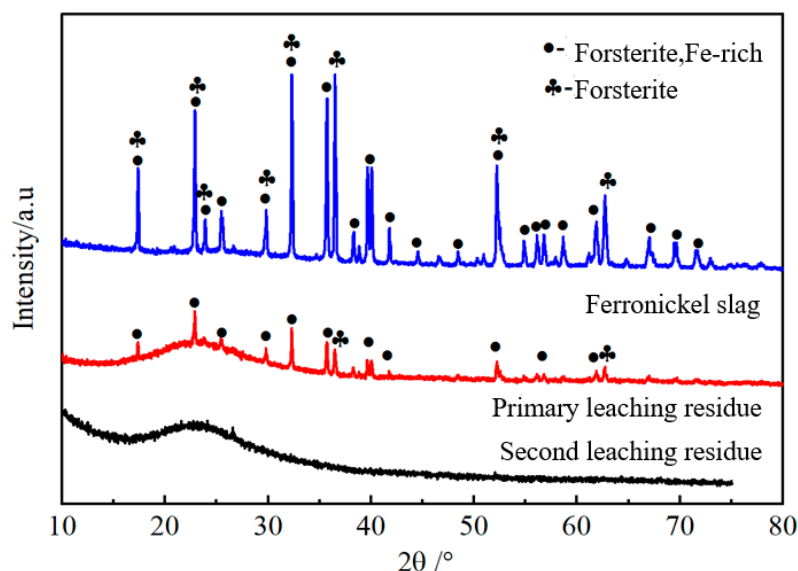
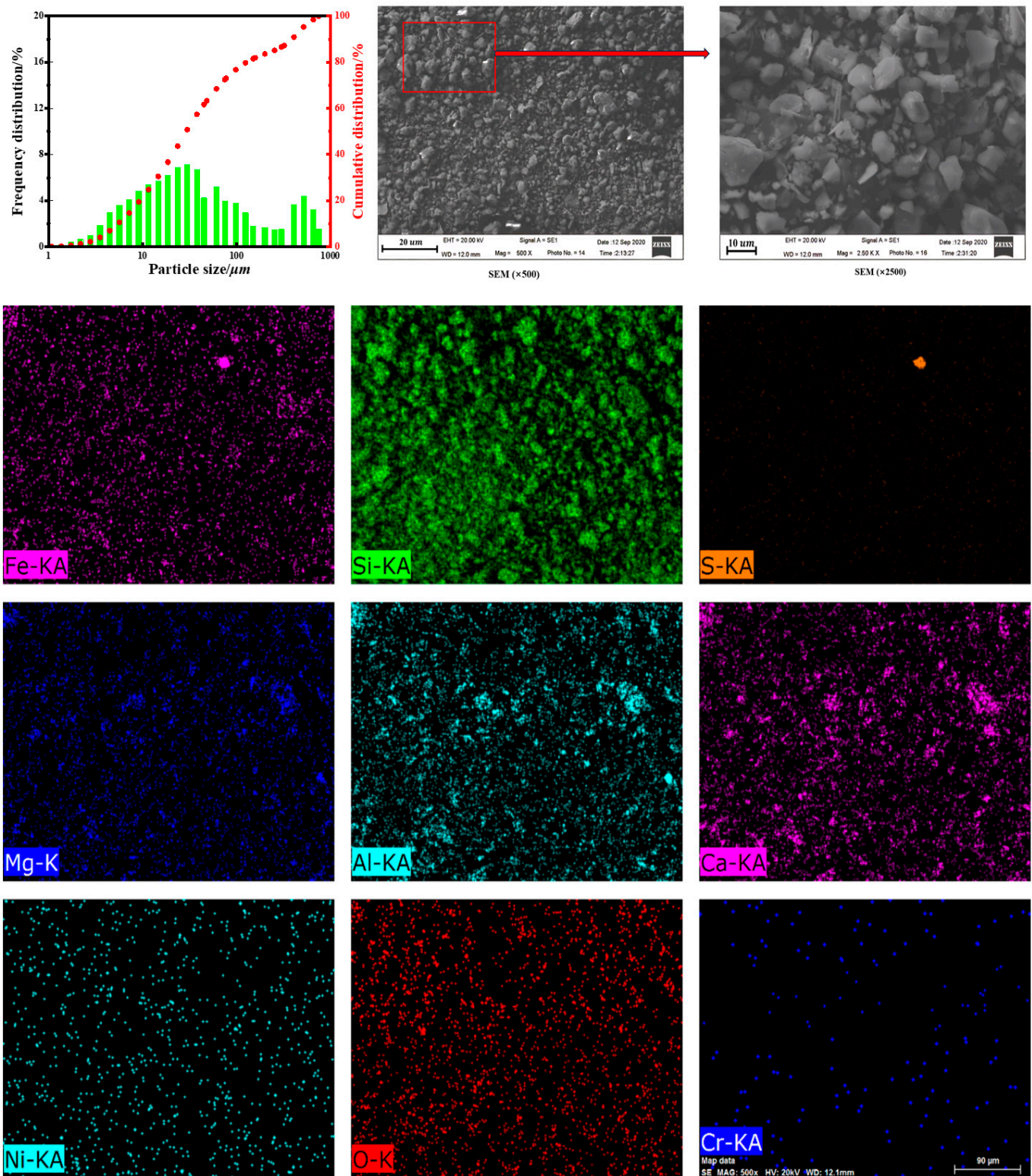
**Figure 2.** XRD spectra of ferronickel slag before and after acid leaching.

Figure 3 illustrates the particle size distribution and microscopic morphology of the second acid leaching residue. It is evident that the particle size of the leaching residue was uneven and fine, with an average volume particle size of 29.16  $\mu\text{m}$ . The tested BET's specific surface area was as high as 418.86  $\text{m}^2/\text{kg}$ , which was conducive to the subsequent carbothermal reduction reaction. The elemental scanning results of the residue reveal the uniform distribution of Si and O elements across the entire slag grain surface. This occurrence suggests that Si and O were uniformly present in the form of silicon dioxide. In contrast, Fe, Ca, and Mg were localized and mainly present in the form of oxides in specific areas. These local impurities will negatively impact the purity of subsequent silicon carbide powder.

The proximate analysis results and other basic characteristics of the four carbon sources are demonstrated in Table 2 [26–29] and Figure 4. From the proximate analysis, we can see certain differences in carbon content and volatile matter content among the four carbon sources: the carbon content of graphite and coke is comparatively high, and the volatile matter content of coke is very low. As an essential raw material, a carbon source with high carbon content is preferable in order to enhance the efficiency of the carbon thermal reduction reaction. When considering the ash content, the distribution of carbon and fixed carbon in a carbon source with a low volatile matter content is relatively intensive, which is more beneficial to the solid phase reaction. In summary, the impacts of the carbon source on the preparation of SiC are nuanced.

**Table 2.** Proximate analysis of carbon source (wt. %).

Carbon Source	M <sub>ad</sub>	A <sub>ad</sub>	V <sub>ad</sub>	FC <sub>ad</sub>	C <sub>d</sub>
Graphite	1.66	15.18	5.01	78.15	81.47
Coke	0.23	18.01	1.80	79.96	79.54
Active carbon	8.26	17.15	21.84	52.75	61.77
Carbon black	1.13	18.96	7.58	72.33	75.74



**Figure 3.** Particle size distribution (The green column represents the frequency of particle size distribution, the red line is the particle size characteristic curve) and microscopic morphology of the second leaching residue (The areas observed by SEM  $\times 2500$  are framed in red and Fe-KA, Si-KA, S-KA, Mg-K, Al-KA, Ca-KA, Ni-KA, O-K, and Cr-KA Fe-KA, Si-KA, S-KA, Mg-K, Al-KA, Ca-KA, Ni-KA, O-K, and Cr-KA is the result of element surface scanning for the area in the red box).

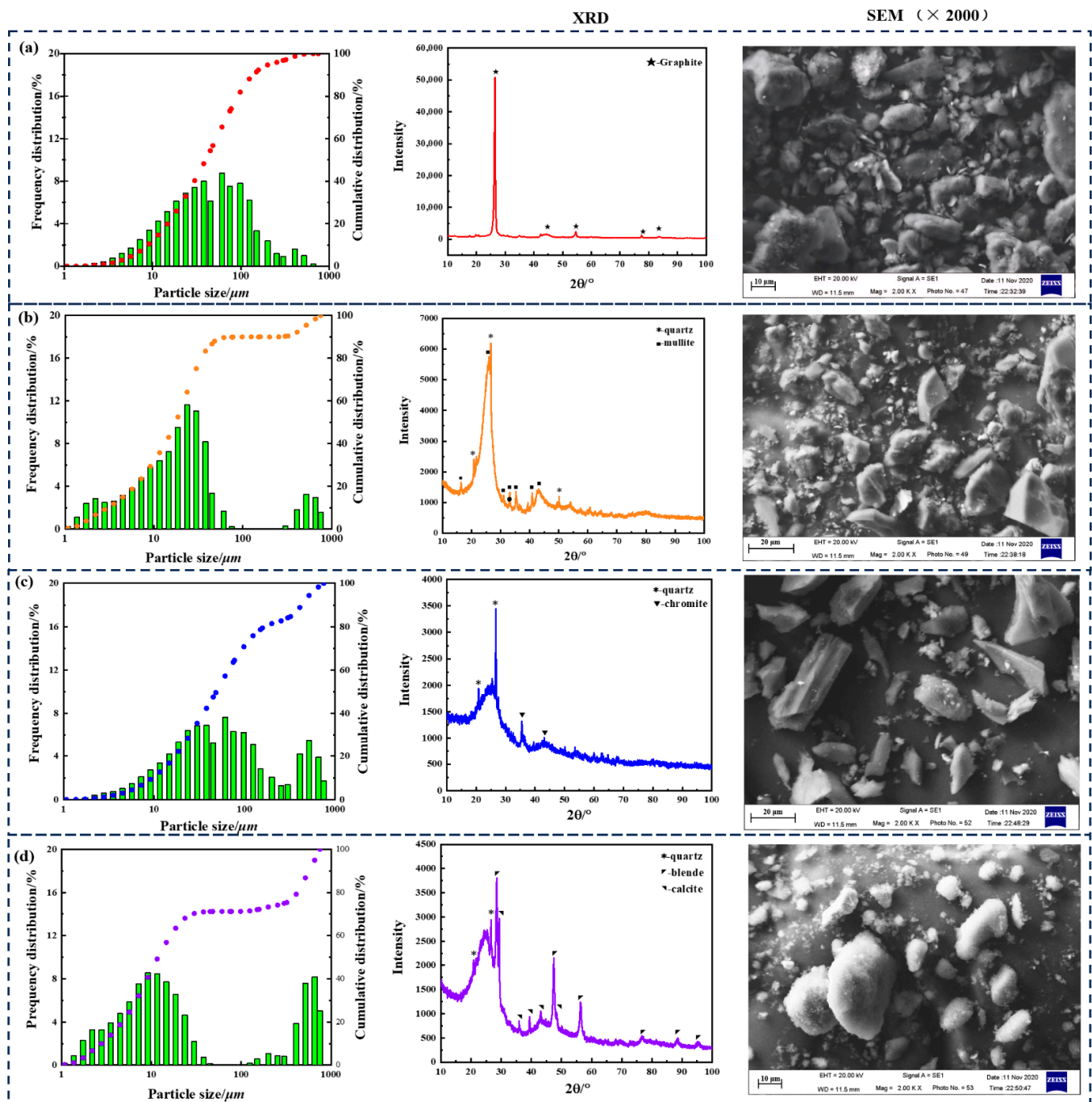


**Figure 4.** Basic characteristics of different carbon sources: (a) graphite, (b) coke, (c) active carbon, (d) carbon black.

As can be seen from Figure 4, the particle size distributions of the four carbon sources were relatively broad. The average particle sizes ( $d_{50}$ ) of graphite powder, coke, activated carbon and carbon black were 39.85  $\mu\text{m}$ , 17.40  $\mu\text{m}$ , 48.68  $\mu\text{m}$  and 11.87  $\mu\text{m}$ , respectively. The smaller the carbon source size, the more favorable for the formation of SiC powder. From the perspective of the reactant size, the selection of a carbon source is reasonable. According to SEM, the four carbon sources were all irregularly shaped particles. The graphite consisted of irregular flake aggregates and the coke comprised irregular polygonal particles, while most of the activated carbon particles were columnar with a small amount of fine debris. The carbon black exhibited the presence of spherical powder, the surfaces of which microspheres were unsmooth and had some fine powder adhering to them.

According to XRD, the mineral phase compositions of the four carbon sources varied. The mineral phase of graphite powder was mainly graphite, while the mineral phase for coke was mainly quartz and mullite. For activated carbon, quartz and chromite were the dominant mineral phases. Quartz, blende and calcite were the primary mineral phases in carbon black. Taken together, the graphite carbon was mainly crystalline carbon, while the carbon in the coke, activated carbon and carbon black were primarily present in the form of amorphous phase. Therefore, due to the relatively high amorphous carbon content, the coke and carbon black were theoretically more reactive during carbothermal reaction.

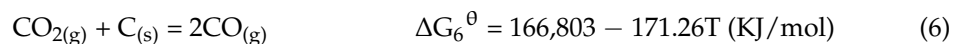
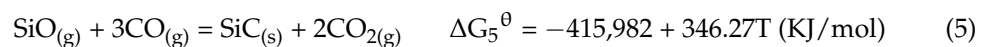
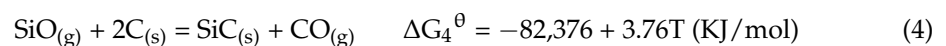
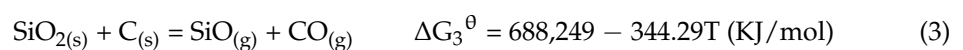
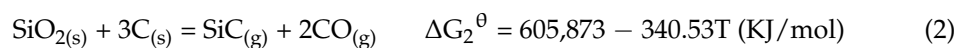
The XRF analysis results of the four carbon sources are presented in Table 3. This shows that among the four carbon sources, Si was the inorganic mineral element with the highest content, which is a benefit to the preparation of SiC powder. Carbon black exhibited relatively high levels of ZnO and TiO content. Activated carbon, on the other hand, showed higher contents of Fe<sub>2</sub>O<sub>3</sub> and CaO. In contrast, coke and graphite ash contained significantly higher levels of Al<sub>2</sub>O<sub>3</sub>. Al<sub>2</sub>O<sub>3</sub> and CaO can be melted at low temperatures to generate a liquid phase, which is helpful in promoting the synthesis of SiC, but these impurities will directly impact the quality of the final SiC product, increasing the difficulty of subsequent purification.

**Table 3.** XRF analysis of ash composition from different carbon sources (wt. %).

Oxide	SiO <sub>2</sub>	Al <sub>2</sub> O <sub>3</sub>	Fe <sub>2</sub> O <sub>3</sub>	CaO	K <sub>2</sub> O	ZnO	MgO	TiO <sub>2</sub>	SO <sub>3</sub>	P <sub>2</sub> O <sub>5</sub>	Others
Graphite	46.781	25.872	8.085	5.753	5.332	2.464	2.042	1.361	0.832	0.626	0.852
Coke	49.634	29.176	11.203	3.805	0.781	0.483	0.913	1.441	0.872	0.804	0.888
Active carbon	30.364	10.742	20.651	5.340	0.721	7.159	2.774	10.213	1.203	10.411	0.422
Carbon black	41.781	2.763	2.414	12.313	0.764	27.192	1.582	0.345	9.764	0.602	0.480

### 3.2. Thermodynamic Analysis

The process of the preparation of SiC via carbothermal reduction involves numerous reactions [30,31], and the dominant reactions that may occur are displayed as Equations (2) to (6). The relationship between the standard Gibbs free energy  $\Delta G^\theta$  and the temperature T of different reactions is shown in Figure 5.



As listed above, SiO<sub>2</sub> (s) first reacts with C (s) to produce gaseous SiO and CO, then a portion of the SiO (g) undergoes gas–solid reaction with C (s), abiding by reaction (4), generating a SiC pellet centered on the reacted carbon granule. Consequently, the shape and size of the formed SiC depend on the morphology and dimension of the reacted carbon. From this perspective, tiny carbon granules are a necessary precondition for the manufacturing of ultra-fine SiC; meanwhile, hindering the growth of SiC at high temperatures is also inherently important. Alternatively, some SiO (g) engages in a gas–gas reaction with CO, as described in Equation (5), transforming into SiC (s) and CO<sub>2</sub>. Furthermore, according to reaction formula (6), the unstable CO<sub>2</sub> easily reacts with C at high-temperatures and readily converts into CO.

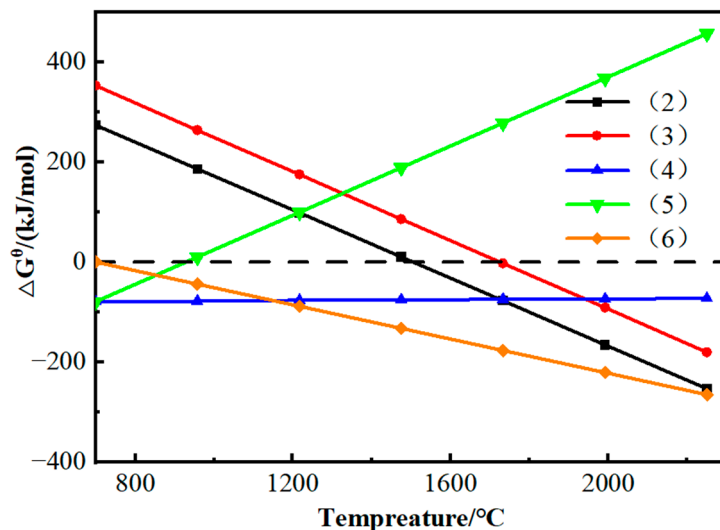
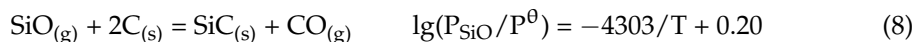


Figure 5.  $\Delta G^\theta$ -T plots for the dominant reactions in the preparation of SiC.

According to Figure 5, the absolute value of  $\Delta G^\theta$  in Equation (4) is greater than that in reaction (5), indicating that reaction (4) is more likely to occur than reaction (5) at the same temperature. Considering that CO is both the outcome in reaction (4) and the reactant in reaction (5), the synthesis process can be regulated by controlling the partial pressure of CO in the reaction system. Additionally, since reaction (5) is more susceptible to temperature than reaction (4), when the process unfolds in a closed environment, the reaction equilibrium constant is likely to change by an order of magnitude with varying temperatures, resulting in a continuous increase in the quantity and partial pressure of CO with the proceeding reaction. Therefore, reactions (4) and (5) can be controlled by regulating the reaction temperature and CO partial pressure, so as to adjust the size and morphology of the obtained SiC. It is worth mentioning that although an increase in temperature is more conducive to the progress of the carbothermal reduction reaction, it also tends to accelerate the volatilization of SiO at the same time. Accordingly, the reasonable theoretical temperature of SiC synthesis should be 1506~1750 °C.

In order to disclose the mechanism of the influence of gaseous SiO over SiC synthesis, the equilibrium partial pressure of SiO gas at different temperatures is gained by theoretical calculation, defining  $P_{CO} = P^\theta$  (where  $P^\theta$  is the standard atmospheric pressure). The curve between  $\lg P_{SiO}/P^\theta$  and  $T^{-1}$  is plotted according to Equations (7)–(10), as shown in Figure 6.



Since the reactant  $\text{SiO}_2$ , C, and outcome SiC in reaction (2) are all pure solids, and  $P_{CO} = P^\theta$ , as well as

$$\Delta G_2^\theta = 605,873 - 340.53T = 0 \quad (11)$$

It can be deduced that the initial reaction temperature for reaction (2) is  $T_{\text{begin}} = 1779$  K (1506 °C). When  $T > T_{\text{begin}}$ , and  $P_{CO} = P^\theta = 101.325$  kPa,  $\text{SiO}_{2(s)}$  and  $\text{C}_{(s)}$  will react to produce  $\text{SiC}_{(s)}$ . As described in Figure 6, when  $\text{SiO}_2$  is reduced by C to create SiC, the partial pressure of SiO (g) in the system is relatively high, indicating a higher content of SiO (g) in the gas phase. Reaction (10) begins at 1871 K (1598 °C), and the equilibrium partial pressure of SiO (g) in reaction (10) gradually reduces with an increasing temperature. In the high-temperature region from 513 °C to 1614 °C, the equilibrium partial pressure of

SiO (g) in reaction (9) exceeds that in reaction (10), whereas the equilibrium partial pressure of SiO (g) in reaction (8) is very low, and increases very slowly as the temperature rises. The equilibrium partial pressure of SiO (g) in reaction (7) also increases rapidly with the temperature increase. Considering the crucial impact of the amount of carbon on the yield and purity of SiC, the dosage of the carbon source needs to be precisely controlled during batching. A reasonably excessive amount of carbon proves to be advantageous for reaction promotion, with its primary functions being: (1) to facilitate a thorough reaction between SiO<sub>2</sub> and C; (2) to augment the contact area between SiO<sub>2</sub> and C, thereby accelerating the reaction rate; (3) to inhibit the coalescence of resulting SiC particles. However, unnecessary carbon consumption is not only a waste of resources, but also prolongs the time required for subsequent decarbonization, posing the risk of the oxidation and purity reduction of SiC.

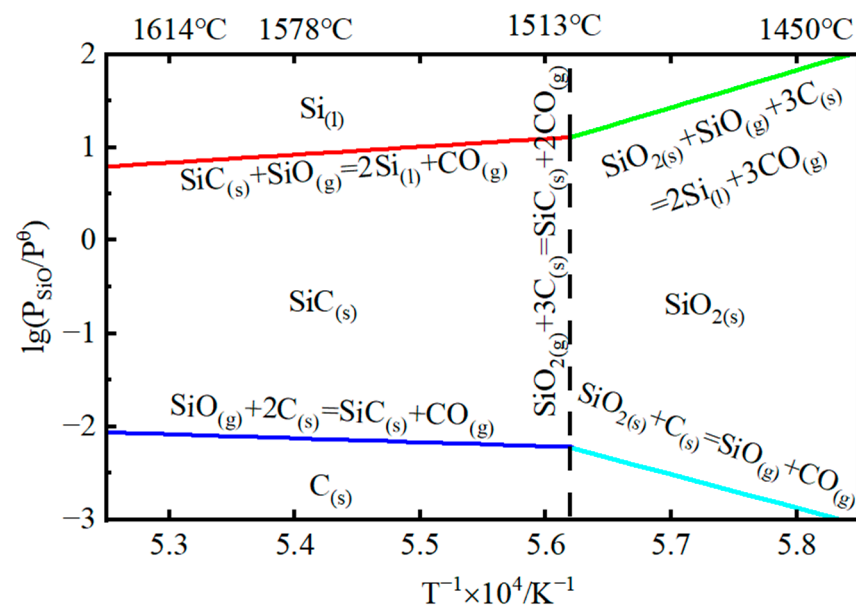


**Figure 6.** Condensed phase in Si–C–O system.

### 3.3. Synthesis of SiC Powder

Figure 7 depicts the XRD patterns of the SiC prepared under different conditions. It is evident from Figure 7a that the diffraction peaks of the prepared products from the four carbon sources appear at 35.6°, 41.4°, 59.9°, and 71.7°, corresponding to the (111), (200), (220), and (311) crystallographic planes of 3C-SiC, respectively. These are close to the value of the standard PDF card of 3C-SiC (PDF#291129), indicating that SiC has been successfully produced from the above four carbon sources, and the prepared SiC belongs to the  $\beta$ -SiC crystal form. When graphite and coke are used, we see a weak characteristic diffraction peak of ferrosilicon (Fe<sub>3</sub>Si) in the XRD spectra of corresponding SiC, which is related to the presence of a certain amount of iron oxides in both silicon and carbon sources. The Fe<sub>3</sub>Si is the reactant of Fe<sub>2</sub>O<sub>3</sub> and SiO<sub>2</sub> at high temperatures. When using carbon black as the carbon source, the XRD pattern of the SiC product will still contain a diffraction peak of SiO<sub>2</sub>, which suggests that some SiO<sub>2</sub> in the leaching residue fails to react completely with C, or some generated SiC is partially oxidized at a high temperature. When the carbon source is graphite, the characteristic diffraction peak of C remains in the SiC's XRD pattern, which reveals that graphite C is minimally active despite a high fixed carbon content, and resulting in a carbon residue. In summary, when graphite and coke are used, the strength of the diffraction peak of SiC in the products is relatively stronger, and the half-peak width of SiC is comparatively narrower, while the impurity peak strength is weak. Combining this finding with the source and price advantages, we see that coke is an ideal carbon source.

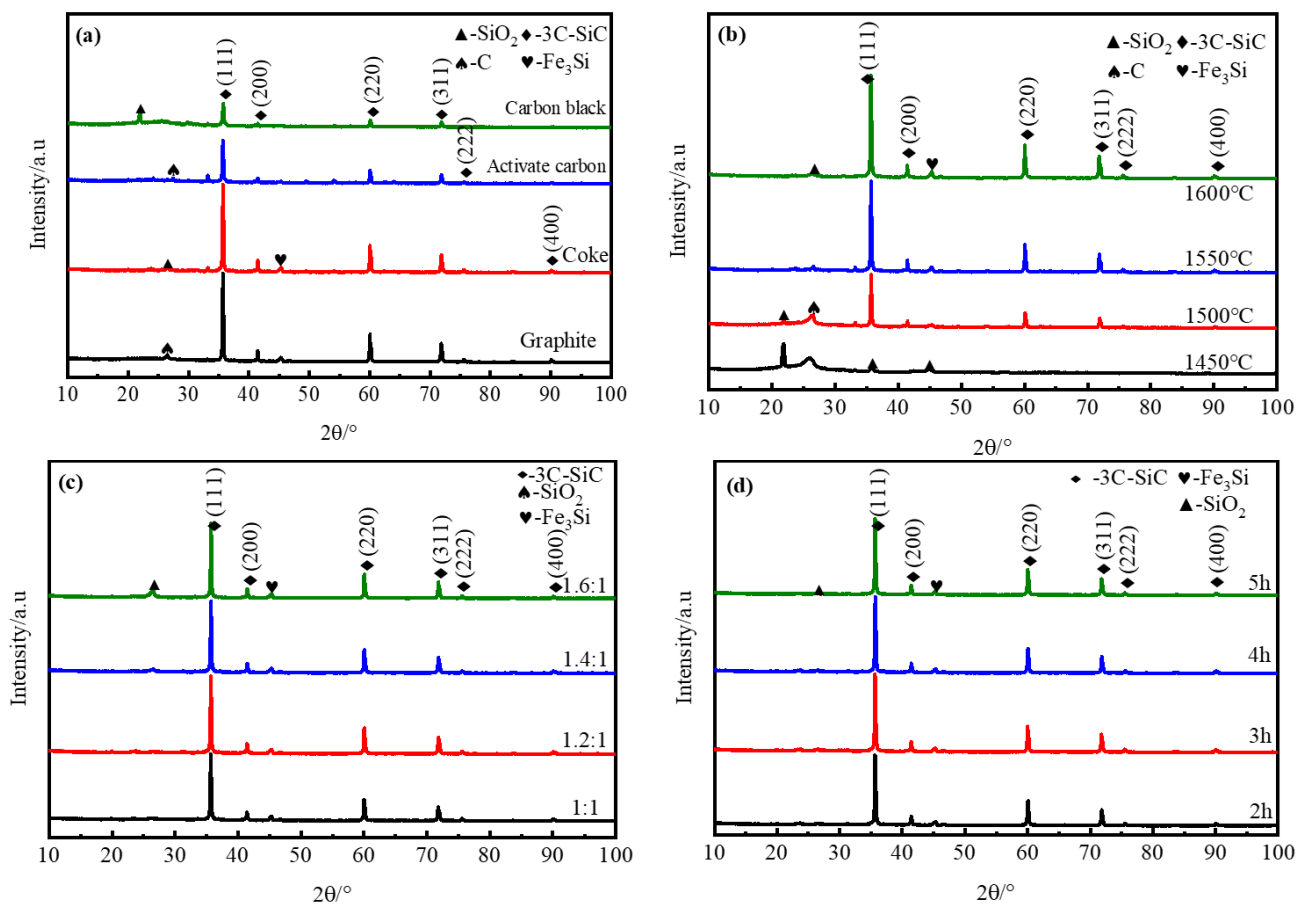


**Figure 7.** XRD analyses of SiC synthesized under different conditions: (a) different carbon sources—carbon mass ratio, 1.4:1; reaction temperature, 1550 °C; reaction time, 5 h; (b) different reaction temperature—coke mass ratio, 1.4:1; reaction time, 5 h; (c) different coke mass ratios—reaction temperature, 1600 °C; reaction time, 5 h; (d) different reaction times—coke mass ratio, 1.2:1; reaction temperature, 1660 °C.

Figure 7b presents the XRD diagram of SiC prepared at different temperatures using coke as the carbon source. It is illustrated that as the reaction temperature increases, the peak intensity of SiO<sub>2</sub> gradually diminishes, while the SiC peak steadily grows, and this is characterized by a strong and sharp primary diffraction peak, directing the formation of highly crystalline SiC. The weak diffraction peaks of Fe<sub>3</sub>Si changed little when the temperature varied, as is presented in the XRD pattern of SiC. Generally, the SiC content of the powder synthesized at 1600 °C is the highest, suggesting the best effect.

The effects of the mass ratio of coke to leaching slag on the SiC are illustrated in Figure 7c. This displays that the optimal mass ratio of coke to leaching slag is 1.2:1, in which case, the diffraction peak of quartz in the synthesized SiC powder is the weakest, while the diffraction peak intensity of SiC is the strongest, which further confirms that excessive carbon will obstruct the synthesis of SiC and lead to a reduction in SiC purity.

As observed in Figure 7d, with the extension of the synthesis time, the diffraction peak intensity of SiO<sub>2</sub> initially decreases and then increases, while the SiC diffraction peak increases at the beginning and finally decreases. At a synthesis time of 3 hours, the SiO<sub>2</sub> diffraction peak of the SiC is the weakest, after which the peak extends with time, suggesting that the reaction time should be regulated within a certain range, as too short is insufficient for complete reacting, while the SiC is likely to be reversely oxidized to SiO<sub>2</sub> and C if it stays in a high-temperature environment for too long. The optimal reaction period for preparing high-purity SiC powder is determined to be 3 hours.

### 3.4. Synthesis Mechanism of SiC

Temperature is one of the most critical factors affecting the purity of SiC powder prepared by the carbon–thermal reduction method [32,33]. Figure 8a shows the FTIR spectrum of SiC powder prepared at different reaction temperatures. It shows that the characteristic peaks at  $3441\text{ cm}^{-1}$  and  $1631\text{ cm}^{-1}$  are caused by the stretching and bending vibrations of -OH. These -OH groups have a dual origin: one from the atmospheric water vapor on the SiC particles, and the other from the hydrogen bonds formed between water molecules and the O in  $\text{SiO}_2$ , which are connected with the polarity of the residual  $\text{SiO}_2$  on the surface of SiC. The peak at  $2342\text{ cm}^{-1}$  belongs to the  $\text{CO}_2$  absorption bond, which is induced by the inclusion of air in the tested sample. The peak at  $1402\text{ cm}^{-1}$  is generated by C–H bending vibration. The peaks located at  $790\text{ cm}^{-1}$  and  $479\text{ cm}^{-1}$  are the symmetric contraction vibration peak and bending vibration peak of Si–O, respectively, and the two characteristic peaks are very prominent at  $1450\text{ }^\circ\text{C}$ , indicating the presence of unreacted  $\text{SiO}_2$  in the product. The characteristic peak at  $1100\text{ cm}^{-1}$  is the anti-symmetric telescopic vibration peak of Si–O–Si. It is noteworthy that at  $1500\text{ }^\circ\text{C}$ , the Si–O–Si characteristic peak is on the right of  $1100\text{ cm}^{-1}$ , and the intensity of the peak is lower than that of the Si–O characteristic peak at  $477\text{ cm}^{-1}$ , whereas the Si–O characteristic absorption peak does not exist at  $790\text{ cm}^{-1}$ . When the temperature is higher than  $1550\text{ }^\circ\text{C}$ , the  $\text{SiO}_2$  characteristic peaks at  $790\text{ cm}^{-1}$  basically disappear, indicating no  $\text{SiO}_2$  in the product. The peak near  $1100\text{ cm}^{-1}$  corresponds to the characteristic peak produced by SiC. In summary, as temperature rises, the  $\text{SiO}_2$  characteristic peak progressively diminishes, which indirectly proves that the SiC content of powder gradually increases with the rising temperature.

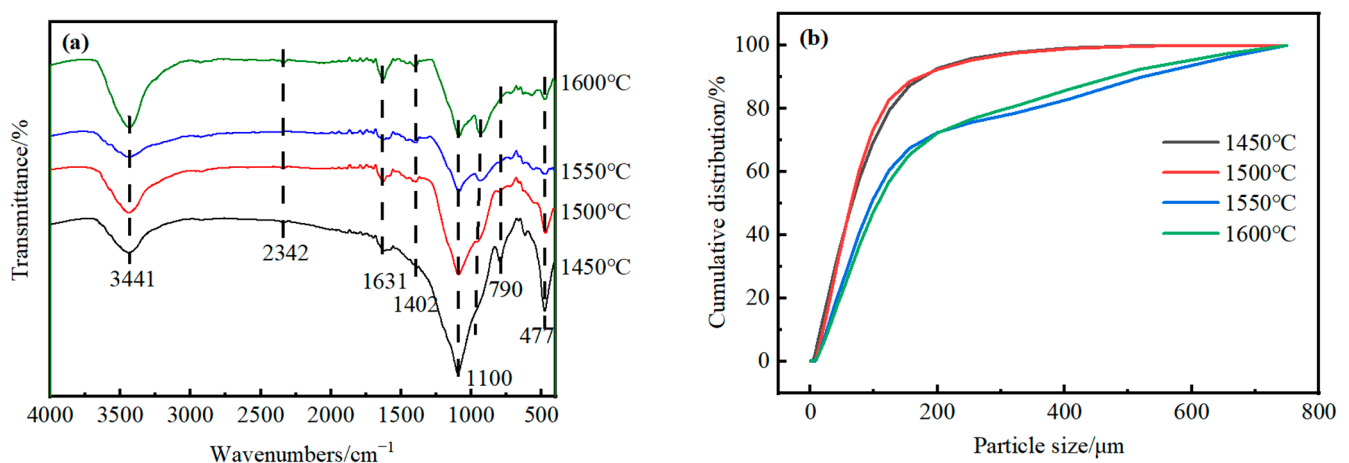


**Figure 8.** Characteristics of SiC powders prepared at different reaction temperatures; coke mass ratio, 1.4:1; reaction time, 5 h: (a) FTIR spectra and (b) particle size analysis.

Figure 8b demonstrates that the prepared SiC powders reached the micron size range, and the particle sizes enlarged progressively with the rising of temperature, with the average particle size increasing from  $65.54\text{ }\mu\text{m}$  at  $1450\text{ }^\circ\text{C}$  to  $105.87\text{ }\mu\text{m}$  at  $1600\text{ }^\circ\text{C}$ . At  $1450\text{ }^\circ\text{C}$ , most leaching residue had not yet reacted, and the particle size reflected in the figure is the dimension of the  $\text{SiO}_2$  in leaching slag. At  $1500\text{ }^\circ\text{C}$ , a small amount of SiC powder had gradually been generated, but the crystallization degree of SiC was very low and the crystals were in the nucleation stage, according to the low reaction temperature, so the particle size was relatively fine. When the temperature reached  $1550\text{ }^\circ\text{C}$ , most of the  $\text{SiO}_2$  in the slag reacted with carbon, and the SiC continued to nucleates and grew slowly, hence the SiC crystal size increasing. When the reaction temperature increased to  $1600\text{ }^\circ\text{C}$ , the nucleated SiC grew rapidly, the crystallinity kept enlarging, and the particle size also increased.

Figure 9 presents the scanning electron microscope (SEM) diagrams of SiC powders prepared at varying reaction temperatures. The powders prepared at  $1450\text{ }^\circ\text{C}$  were mainly

composed of particles with clear boundaries and relatively regular shapes, and the geometric configurations of these particles were primarily spherical and angular polygons. The larger spherical particles were mainly composed of carbon and silicon dioxide, presumably a transition-state substance formed under high temperatures, while the polygonal particles mainly belonged to pyrolytic coke and nickel–iron slag, some of which were covered with a fine pyrolytic carbon grain. According to EDS, there was almost no SiC in the powder prepared at 1450 °C, suggesting that the carbothermal reaction rarely occurred at 1450 °C. When synthesized at 1500 °C, the products were still predominantly spherical and irregular polygons, but covered by floccules to a varying degree, and there was a certain degree of cross-linking between the particles. EDS analysis further evinced that the covering layer was mainly composed of C, Si, and O, and the atom ratio of Si to O was close to 1:1, suggesting the emergence of SiO. Combined with the reduction of on-site carbon content, it can be inferred that SiO<sub>2</sub> and C started to react at 1500 °C to generate CO and CO<sub>2</sub>, and formed a small amount of SiC. Furthermore, the surface of the reaction outcome at 1500 °C was almost overlapped with floc, composed of SiC and the incomplete reacting product of leaching residue and carbon. It is clear that a large amount of SiC crystal has formed at 1550 °C, some of which was generated around the leaching slag particle. At 1600 °C, the major composition of the produced powder was high-purity SiC, containing a small amount of residual carbon and trace SiO<sub>2</sub> which might be derived from the oxidation of SiC at high temperatures. The powder particles were generally irregular and had pores inside, caused by the escape of the gas originating from the reaction of SiO<sub>2</sub> and C. In addition, the color of the SiC powder changed from light green to dark green with the increase in temperature (as shown in Figure 9).

The crystallization of SiC is a form of heterogeneous nucleation. According to classical crystal nucleation theory [34], because of the notch effect, the new phase preferentially nucleates at the notch of the nucleation promoter. The smaller the notch radius, the lower the nucleation energy, the easier it is to nucleate, and the more stable the nucleus is. In gas-phase nucleation, the formation of a new phase is intricately tied to the degree of gas supersaturation. The supersaturation degree determines the critical radius for crystal nucleation, and as supersaturation increases, this critical radius decreases, making nucleation easier. Simultaneously, the supersaturation of the gas also affects the crystals' nucleation. In accordance with Weimarn's law [35], competition unfolds between the nucleation and growth phases during crystal formation. The swifter the nucleation process, the greater the number of nuclei that emerge before supersaturation subsides, yielding a correspondingly reduced particle size in the resulting crystal. This implies that the crystal nucleation rate increases as the gas supersaturation rises.

It can be inferred that the formation of SiC powder follows both gas–solid and solid–solid reaction mechanisms. As shown in Figure 10a, when the temperature and gas phase partial pressure are satisfied, SiO (g) diffuses to the surface of C particles, and the SiC unevenly nucleates and grows on the surface of carbon particles through reaction (4), forming a SiC layer. The formation of these SiC particles conform to a gas–solid (V-S) reaction mechanism, resulting in a fine particle size, mostly attached to the solid–solid nucleated SiC particles.

Based on reaction kinetics, reaction (4) is a gas–solid reaction that occurs as shown in Figure 10a: on the one hand, SiO diffused to the surface of C particles reacted with C to form SiC and CO; on the other hand, CO molecules desorbed and left the surface of C particles. Despite the fast reaction rate between SiO and C, the overall rate of reaction (4) is controlled by the slowest diffusing gas molecules at the phase interface, and thus the overall rate of gas–solid reaction (4) is relatively slow. Reaction (5) is a homogeneous reaction that occurs at the gas–gas interface; therefore, the overall reaction rate of reaction (5) is higher than that of reaction (4).

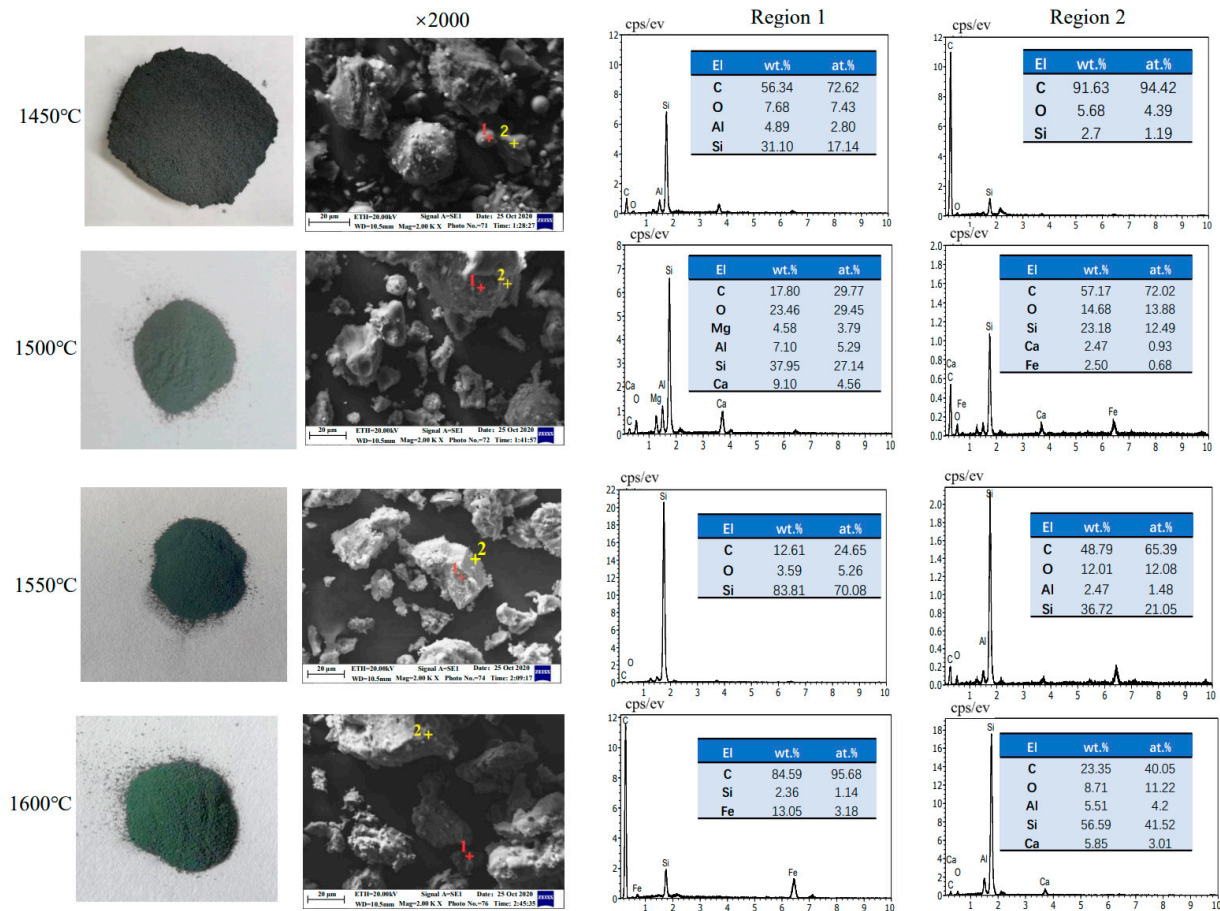


**Figure 9.** SEM images of SiC powders prepared at different reaction temperatures: coke mass ratio, 1:1.4; reaction time, 5 h ((1+) and (2+) are the EDS measuring regions of region 1 and region 2, respectively).

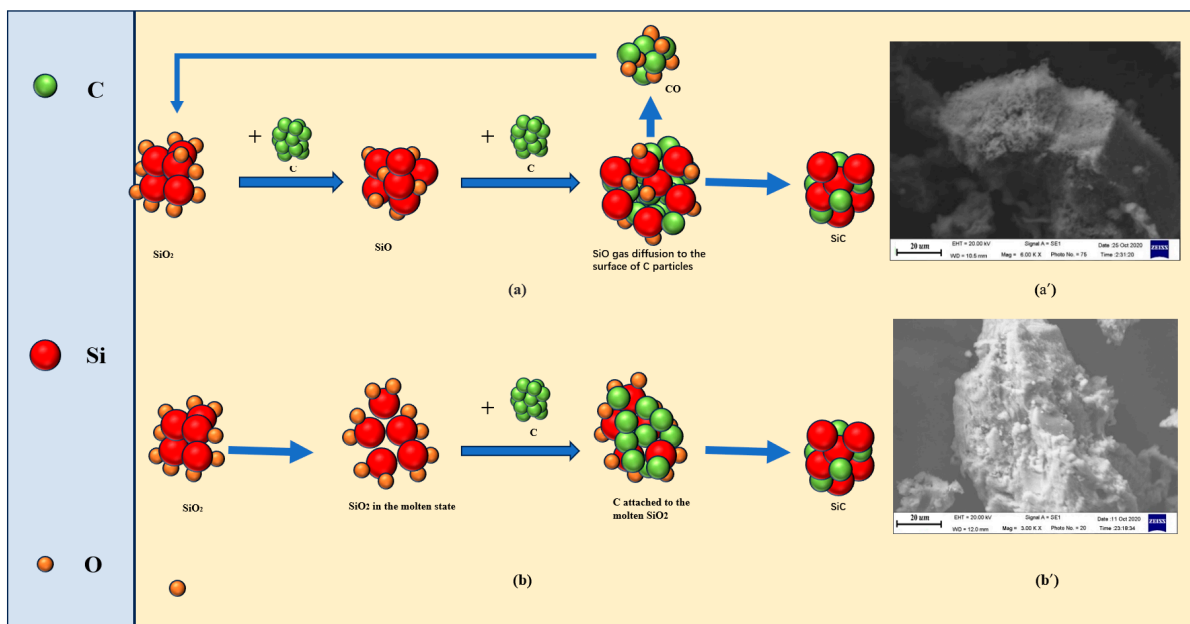


**Figure 10.** Generation mechanism and microscopic morphology of SiC: (a) Gas–solid mechanism. (a') Surface attachment of SiC powder. (b) Solid–solid mechanism. (b') SiC encapsulated by pyrolytic C particles.

During the initial stages of the carbothermal reduction reaction, the leaching slag and C particles are in close proximity, with reaction (3) yielding SiO (g), and the generated SiO(g) reacts with C to form SiC particles through reaction (4). With the progress of the reaction, the SiC generated on the surface of the carbon particles gradually thickens, hindering the diffusion of solid C and the gas SiO; consequently, the reactions (3) and (4) gradually slow down and finally stop, resulting in the incomplete reaction of carbon and manifesting a “carbon core” inside the SiC particles, as shown in Figure 10a'. This phenomenon is particularly pronounced when the size of the carbon particles is substantial [36]. Thereafter, SiC might be generated through a gas–gas reaction (5) between SiO and CO.

In addition, SiC is also generated in situ in the position of SiO<sub>2</sub> of the leaching residue through the solid–solid reaction mechanism (S-S), as shown in Figure 10b. Owing to the poor stability of amorphous silica, leaching slag gradually softens and changes into a molten body at elevated temperatures of 1500 °C. Under this circumstance, the outer coated carbon diffuses into the molten slag gradually, undergoing a solid–solid reaction with SiO<sub>2</sub> as shown in Equation (2), and SiC is gradually generated in situ in slag. As the reaction proceeds, the carbon in the outer layer continues to diffuse inwards and continues reacting with SiO<sub>2</sub>, and the SiC particles nucleate and grow progressively until the SiO<sub>2</sub> in the slag is completely reacted. As a consequence, the SiC particles are encapsulated by aggregates of fine pyrolytic carbon particles of coke, as exhibited in Figure 10b'. The formation of these SiC particles follow the solid–solid reaction mechanism, and their particle size is close to the original particle size of the acid leaching slag.

### 3.5. Purification of SiC Powder

Calcination can eliminate the impurity carbon from the SiC powder by oxidizing the free carbon. The purification effects of SiC calcination are depicted in Figure 11. As shown in Figure 11a, when the calcination time is extended, the LOI of the SiC powder initially rises and then decreases. The optimum carbon removal effect is achieved with a maximum LOI of 22.82% after 4 h calcination. Excessive calcination is likely to result in the surface oxidation of SiC, and the generated silicon oxide film will envelop the SiC and hinder the carbon removal, which is consistent with the findings of Fu [37]. Figure 11b illustrates the variations in LOI of SiC powder when calcinated at different temperatures. It has been reported that [38] the larger the particle size of impurity carbon in SiC powder, the higher the temperature at which significant oxidation begins. In this study, after calcinating at 600 °C for 4 h, the LOI of SiC powder reached 15.72%, indicating the significant oxidation of impurity carbon had already begun. Following calcination at 700 °C, the LOI of powder underwent a substantial increase to 24.40%, and the oxidation of free carbon became more active during this stage. However, when the calcination temperature increased to 800 °C, the LOI of powder slightly decreased to 22.82%. Continuing to raise the temperature to 900 °C resulted in a further reduction of LOI to 18.17%. Theoretically, the increase in calcination temperature should promote the complete oxidation of residual carbon, which leads to a gradual increase in the LOI, and then it leveling off. The experiment results are not in accordance with the theoretical analysis, and the only possible cause is SiC oxidation at high temperatures, causing an increase in the LOI of SiC powder. The equation for the oxidation of SiC is shown in (12).



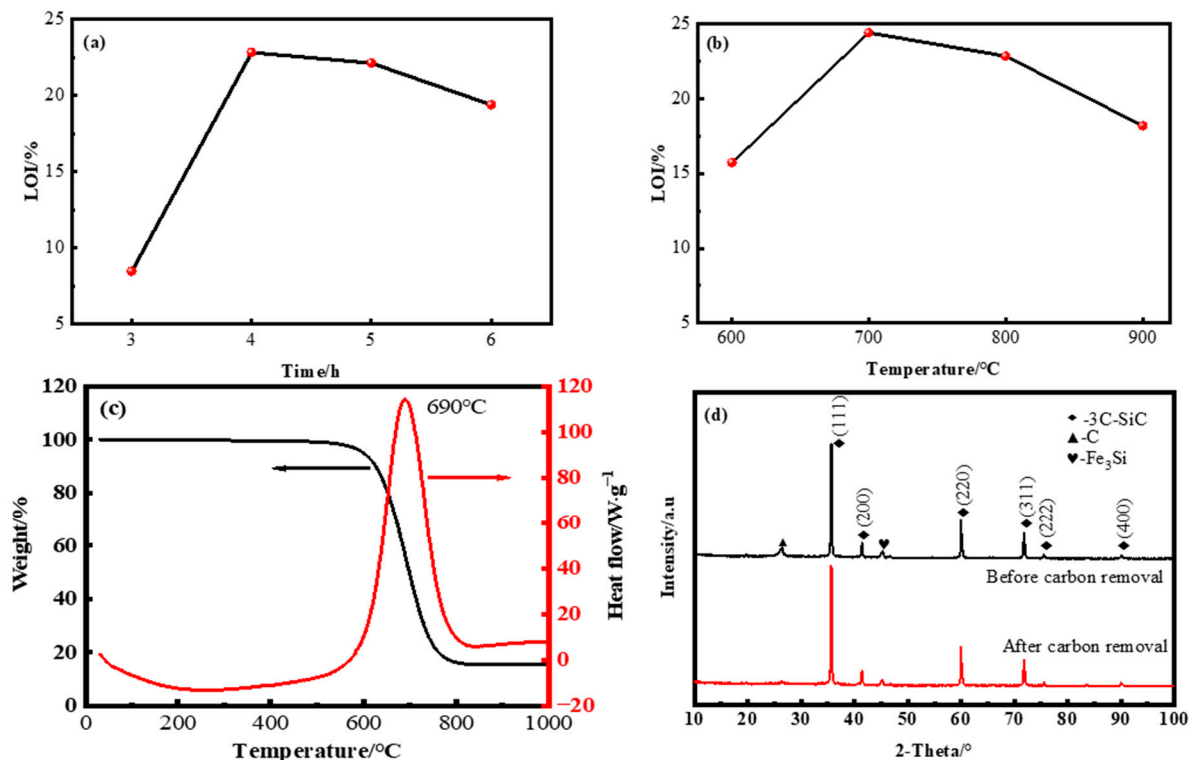


**Figure 11.** Purification by calcination: (a) effect of calcination time on carbon removal; (b) effect of calcination temperature on carbon removal; (c) TG-DSC curves of coke; (d) XRD quantitative analysis of SiC powder before and after carbon removal.

The free carbon in SiC primarily originated from the carbon source, which did not completely react. Figure 11c represents the thermogravimetric curve of the coke. It is clear that, starting from 600 °C, the coke absorbed heat and underwent decomposition, leading to a significant weight loss, which continued until around 800 °C. The pyrolysis rate of the coke was relatively slow at temperatures lower than 600 °C, but as the temperature surpassed 600 °C, the pyrolysis rate rapidly increased before gradually decreasing. Around 690 °C, the decomposition rate of the coke reached its peak. Therefore, to maximize the removal of residual carbon from SiC powder and simultaneously avoid the excessive oxidation of SiC, the recommended calcination temperature is 700 °C.

The XRD patterns for the SiC powder before and after carbon removal are exhibited in Figure 11d. Prior to carbon removal, the dominant crystalline phase in the powder was 3C-SiC, with the presence of a graphite phase. Post carbon removal, the primary crystalline phase in the powder remained 3C-SiC, and the graphite phase had vanished. This signifies that the calcination achieved the intended effect of carbon removal. In addition, the intensity of the SiC diffraction peaks of powder increased, and the peak widths at half height narrowed after calcination, indicating that carbon removal increased the purity of the SiC powder.

The primary characterizations of the final SiC powder is depicted in Figure 12. As shown in Figure 12a, the powder exhibited a green color with a fine particle size. In the SEM image, the presence of SiC whiskers can be observed. According to EDS analysis, only a small quantity of metal element was detected within the powder. In Figure 12b, showing the FTIR spectrum of the powder, the absorption peak at 926 cm<sup>-1</sup> is attributed to the stretching vibration of the Si–C bond; the presence of Si–O–Si symmetric absorption peaks at 473 cm<sup>-1</sup> and 1091 cm<sup>-1</sup> suggests a small amount of amorphous SiO<sub>2</sub> remaining in the powder; the characteristic peaks at 3438 cm<sup>-1</sup> and 1623 cm<sup>-1</sup> are produced by the stretching and bending vibrations of -OH, respectively. The results of the laser particle size analysis in Figure 11c show that the produced SiC falls in the micron size range,

characterized by  $d_{90} = 295.09 \mu\text{m}$  and  $d_{50} = 44.68 \mu\text{m}$ . The quantitative XRD analysis shown in Figure 11d indicates that the SiC content of the powder was 88.90%.

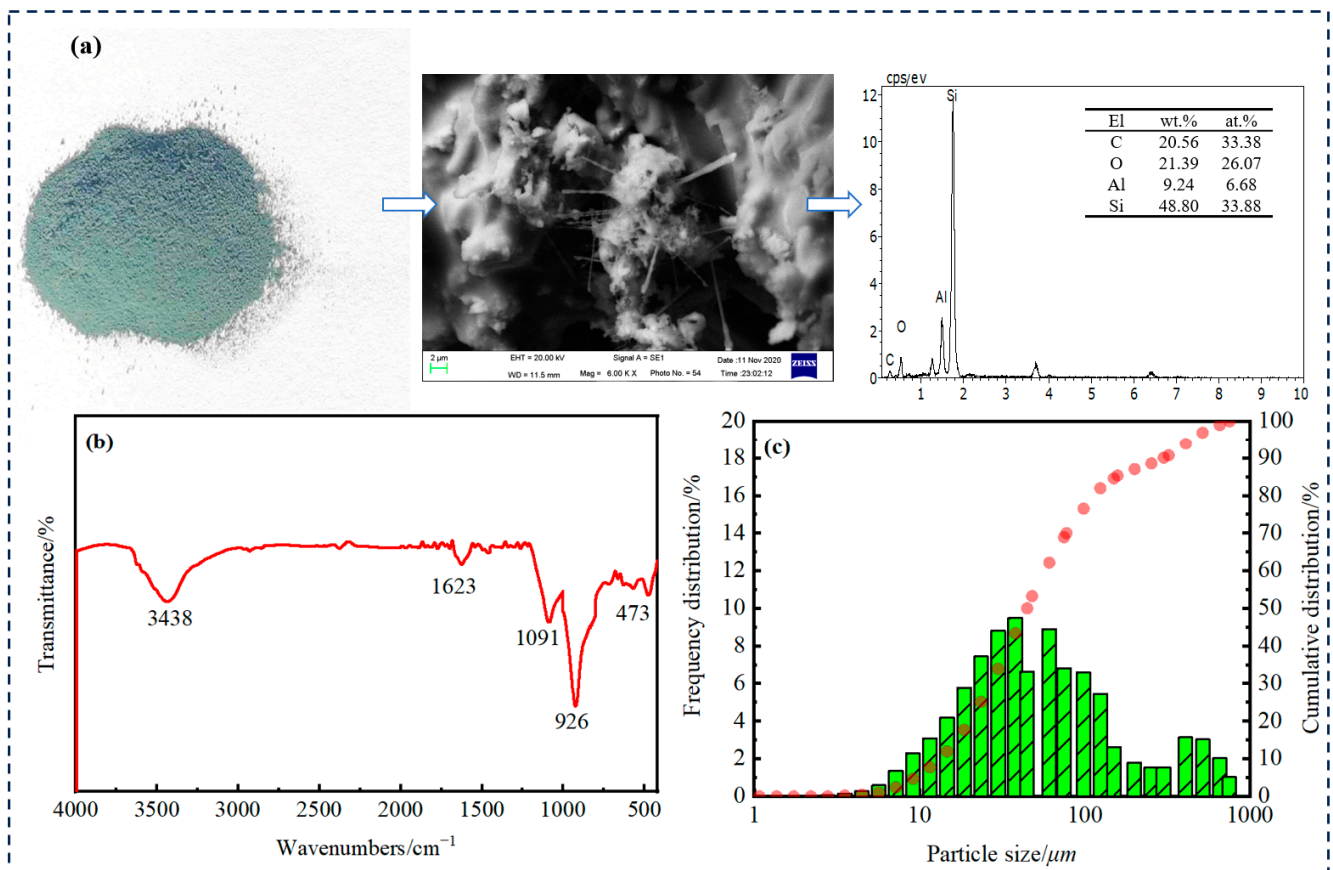


**Figure 12.** Characteristics of final SiC powder: (a) Macro- and micro-morphology; (b) FTIR spectrogram; (c) Particle size distribution.

#### 4. Conclusions

This study presents a systematic investigation of SiC preparation through the carbon thermal reduction method, utilizing the acid leaching residue of ferronickel slag as a silicon source. The objective is to reduce the cost of Si raw material and explore a feasible method for the resource utilization of “silicon-based” acid leaching tailing.

- The acid leaching residue exhibited a high content of amorphous silica, making it an ideal silicon source for the preparation of silicon carbide powder. Coke is the preferable carbon source. Temperature is the most vital factor affecting the preparation of SiC. Increasing the temperature is conducive to improving the reaction rate and shortening the reaction time. The theoretical synthesis temperature of SiC should be above  $1500\text{ }^{\circ}\text{C}$ .
- The optimum conditions for SiC synthesis are as follows: a mass ratio of coke to leaching residue of 1.2:1, a reaction temperature of  $1600\text{ }^{\circ}\text{C}$ , and a synthesis time of 3 h. The optimal carbon removal conditions include a calcination temperature of  $700\text{ }^{\circ}\text{C}$  and a decarbonization time of 4 h. The prepared SiC is characterized by a purity of 88.90%,  $d_{50} = 44.68 \mu\text{m}$ , and a color of green, which reveal that the SiC was a  $\beta$ -SiC crystalline micron powder.
- Using amorphous silica and coke as raw materials, the carbon thermal reduction synthesis of SiC followed both solid–solid and gas–solid reaction mechanisms. The SiC formed according to the solid–solid reaction mechanism nucleated the silica in the leaching slag in situ; as a consequence, its size was close to that of the slag particles.

The SiC generated following the gas–solid reaction mechanism nucleated unevenly on the surface of the carbon particles, and its particles were microfine, mostly attached to the surfaces of the coarse-grained SiC.

**Author Contributions:** Methodology, conceptualization, writing—original draft, X.D.; writing—review and editing, data curation, formal analysis, S.L. Conceptualization, investigation, X.J. Supervision, H.Y. Investigation, T.L. All authors have read and agreed to the published version of the manuscript.

**Funding:** This research received no external funding.

**Data Availability Statement:** Data are contained within the article.

**Acknowledgments:** We would like to express our sincere thanks to the anonymous reviewers for their insightful comments, which helped us improve the quality of this paper.

**Conflicts of Interest:** The authors declare no conflicts of interest.

## References

- Han, F.H.; Zhang, H.B.; Li, Y.C.; Zhang, Z.Q. Recycling and comprehensive utilization of ferronickel slag in concrete. *J. Clean. Prod.* **2023**, *414*, 137–633. [[CrossRef](#)]
- Oktavia, E.K.; Federico, P.; Hee-Jeong, K. Application of steel slags, ferronickel slags, and copper mining waste as construction materials: A review. *Resour. Conserv. Recycl.* **2023**, *198*, 107–175.
- Shang, W.X.; Pang, Z.X.; Xu, F.C.; Tang, H.M.; Rao, M.J.; Li, G.H.; Jiang, T. Preparation of enstatite-spinel based glass-ceramics by co-utilization of ferronickel slag and coal fly ash. *Ceram. Int.* **2021**, *47*, 29400–29409. [[CrossRef](#)]
- Tang, H.M.; Peng, Z.W.; Shang, W.X.; Ye, L.; Luo, J.; Rao, M.J.; Li, J.H. Preparation of refractory materials from electric furnace ferronickel slag and blast furnace ferronickel slag: A comparison. *J. Environ. Chem. Eng.* **2022**, *10*, 107929. [[CrossRef](#)]
- Lin, C.; Lu, S.; Li, Z.M.; Huang, C.D.; Jiang, H.; Peng, B. Recycling of ferronickel slag tailing in cementitious materials: Activation and performance. *Sci. Total Environ.* **2023**, *861*, 160709.
- Gao, Y.H.; Jiang, T.; Xu, Z. Microwave Roasting and Acid Leaching of Vanadium and Chromium from High Chromium Vanadium Slag with CaCO<sub>3</sub>. *Solid State Phenom.* **2019**, *294*, 86–91. [[CrossRef](#)]
- Ahn, N.K.; Shim, H.W.; Kim, D.W.; Swain, B. Valorization of waste NiMH battery through recovery of critical rare earth metal: A simple recycling process for the circular economy. *Waste Manag.* **2020**, *104*, 154–261. [[CrossRef](#)]
- Wang, Y.W.; Chang, X.J.; Chen, M.J.; Qin, W.Q.; Han, J.W. Effective extraction of nickel and cobalt from sintered nickel alloy via reduction roasting and leaching. *Miner. Eng.* **2023**, *203*, 108–336. [[CrossRef](#)]
- Wang, Q.R.; Wang, S.; Ma, X.; Cao, Z.F.; Di, G.K.; Yang, J.; Zhong, H. A Green Cyclic Leaching Process for Low-Grade Pyrolusite via a Recyclable Fe (II) Reductant. *Minerals* **2023**, *13*, 1191–1309. [[CrossRef](#)]
- Yang, J.; Duan, X.Q.; Liu, L.C.; Yang, H.F.; Jiang, X.C. Recovery of Magnesium from Ferronickel Slag to Prepare Magnesium Oxide by Sulfuric Acid Leaching. *Minerals* **2021**, *1*, 1112–1375. [[CrossRef](#)]
- Li, S.H.; Fang, Y.; Cheng, L.F.; Li, Z.C.; Wang, J.H.; Tu, J.Y. Porous silicon carbide ceramics with directional pore structures by CVI combined with sacrificial template method. *Ceram. Int.* **2023**, *49*, 8331–8338. [[CrossRef](#)]
- Li, S.J.; Cui, H.S.; Ma, Q.L.; Liu, X.; Wang, Y.; Shang, L.H.; Zheng, Y.L. The one-step pyrolysis process of rattan-based silicon carbide multiphase ceramics prepared by sol–gel metho. *J. Wood Sci.* **2021**, *67*, 58–67. [[CrossRef](#)]
- Zaitsev, V.S.; Doroganov, A.E.; Doroganov, A.V.; Evtushenko, I.E.; Sysa, K.O. Artificial Ceramic Binders based on Silicon and Silicon Carbide for Silicon–Carbide Refractories in a Nitride Matrix. *Refract. Ind. Ceram.* **2020**, *60*, 439–445. [[CrossRef](#)]
- Chen, Y.; Ding, J.; Deng, C.; Yu, C. Improved thermal shock stability and oxidation resistance of low-carbon MgO–C refractories with introduction of SiC whiskers. *Ceram. Int.* **2023**, *16*, 26871–26878. [[CrossRef](#)]
- Zhang, H.; Tao, B.C.; Den, Q.F.; Zhang, C.Q.; Lyu, B.H.; Nguyen, D.N. Research on Abrasive Water Jet Polishing of Silicon Carbide Based on Fluid Self-Excited Oscillation Pulse. *Charact. Micromach.* **2023**, *14*, 852–1104. [[CrossRef](#)] [[PubMed](#)]
- Ouyang, C. Application on Research of Silicon Carbide Material in Nonferrous Metallurgy. *Sustain. Min. Metall.* **2019**, *35*, 9–11.
- Wang, J.P.; He, D.H.; Zhao, W.Y. Research Status and Application Prospect of Silicon Carbide Materials. *Equip. Electron. Prod. Manuf.* **2018**, *47*, 23–26.
- Lao, X.B.; Xu, X.Y.; Jiang, W.H.; Yang, J.; Niao, L.F. Influences of Al metal and Al–Si alloys on in-situ synthesis of SiC nanowhiskers in porous Al<sub>2</sub>O<sub>3</sub>–SiC composites obtained by carbothermal reduction. *J. Alloys Compd.* **2020**, *854*, 157–182.
- Li, F.H.; Guo, Z.Y.; Su, G.; Guo, C.B.; Sun, G.J.; Zhu, X.L. Preparation of SiC from acid-leached coal gangue by carbothermal reduction. *Int. J. Appl. Ceram. Technol.* **2018**, *15*, 56–128. [[CrossRef](#)]
- Guo, X.; Zhang, L.; Yan, L.; Yan, H.; Zhu, L. Preparation of silicon carbide using bamboo charcoal as carbon source. *Mater. Lett.* **2009**, *64*, 331–333.
- Wang, X.F.; Liu, K.; Nie, D.; Jun, M.; Meng, F.J.; Xing, P.X. Effects of different carbon sources on the preparation of silicon carbide from silicon micro powder. *Ferro-Alloys* **2020**, *51*, 10–14.

22. He, J.F.; Zhang, H.J.; Ge, T.; Liu, J.T.; Wu, W.H. Research progress in preparation methods of SiC porous ceramics. *Refractories* **2020**, *54*, 163–171.
23. Lu, P.; Jin, Z.; Cui, L.; Xu, G.; Wu, R. Effect of raw material size on the synthesis of silicon carbide. *CIESC J.* **2021**, *72*, 2300–2308.
24. Liu, C.L. The Study on the Comprehensive Utilization and Recovery of Valuable Components from Electric Furnace Nickel-Iron Slag. Master's Thesis, University of Science and Technology Beijing, Beijing, China, 2018.
25. GB/T 34231-2017; Coal. Determination of Loss on Ignition for Coal Combustion Residues. National Standardization Administration of China: Beijing, China, 2017.
26. GB/T 3521-2008; China Nonmetallic Mineral Products Standard Technical Committee. Method for Chemical Analysis of Graphite. National Standardization Administration of China: Beijing, China, 2008.
27. GB 2001-2013; Coking Chemicals. Coke-Determination of Proximate Analysis. National Standardization Administration of China: Beijing, China, 2001.
28. GB/T 3780.10-2017; Rubber and Rubber Products. Carbon Black—Part 10: Determination of Ash. National Standardization Administration of China: Beijing, China, 2017.
29. GB/T 7702.15-2008; China North Industries Group Corporation Limited. Test Method for Granular Activated Carbon from Coal-Determination of Ash Content. National Standardization Administration of China: Beijing, China, 2008.
30. Li, X.W.; Qv, D.L.; Li, Z.J.; Wu, F.; Xu, N. Study on the Thermodynamics and Characterization of Synthesizing SiC Whiskers. *J. Synth. Cryst.* **2013**, *42*, 2160–2169.
31. He, T.Y.; Bai, J.G.; Zhao, Q.; Liang, L.D.; Huang, C.Q.; Huang, R.; Wang, R.X. Study on silicon carbide whisker formation mechanism. *J. Shaanxi Univ. Sci. Technol.* **2022**, *40*, 39–123.
32. Sun, H.G.; Li, H.X.; Si, Y.C.; Du, Y.H.; Zhao, S.X.; Shang, L.Q.; Xia, M. Effect of heat treatment temperature on properties of SiC-MgAl<sub>2</sub>O<sub>3</sub>-Al composites. *Refractories* **2023**, *57*, 390–396.
33. Wang, L.; Li, J.H.; Li, H.M.; Bao, G.P.; Zhang, H. Effect of process temperature and performance of silicon carbide film layers made via CVD strategy. *China High New Technol.* **2023**, 99–101.
34. Fu, G.Z. Research description of two kinds of nucleation of crystals theory. *Shandong* **2013**, *36*, 18–22.
35. Weimer, A.; Nilsen, K.; Cochran, G. Kinetics of carbothermal reduction synthesis of beta silicon carbide. *Aiche J.* **1993**, *39*, 493–503. [[CrossRef](#)]
36. Yoon, S.; Ou, J.K.; Seung, M. Formation of Silica-Coated Carbon Powder and Conversion to Spherical  $\beta$ -Silicon Carbide by Carbothermal Reduction. *J. Am. Ceram. Soc.* **2002**, *85*, 2134–2136.
37. Fu, Z.C. The Research on Removing Carbon and Iron from Industrial Silico Carbide. Master's Thesis, Lanzhou University of Technology, Lanzhou, China, 2013.
38. Zhao, Y.F.; Liu, Y.; Zhao, X.Y. Research progress on removing carbon and iron technology from silicon carbide powder. *Guangzhou Chem. Ind.* **2016**, *44*, 7–9.

**Disclaimer/Publisher's Note:** The statements, opinions and data contained in all publications are solely those of the individual author(s) and contributor(s) and not of MDPI and/or the editor(s). MDPI and/or the editor(s) disclaim responsibility for any injury to people or property resulting from any ideas, methods, instructions or products referred to in the content.